

Pseudogap and its connection to particle-hole asymmetry electronic state and Fermi arcs in cuprate superconductors

Huaisong Zhao, Lülin Kuang, and Shiping Feng*

Department of Physics, Beijing Normal University, Beijing 100875, China

The particle-hole asymmetry electronic state of cuprate superconductors and the related doping and temperature dependence of the Fermi arc length are studied based on the kinetic energy driven superconducting mechanism. By taking into account the interplay between the SC gap and normal-state pseudogap, the essential feature of the evolution of the Fermi arc length with doping and temperature is qualitatively reproduced. It is shown that the particle-hole asymmetry electronic state is a natural consequence due to the presence the normal-state pseudogap in the particle-hole channel. The Fermi arc length increases with increasing temperatures below the normal-state pseudogap crossover temperature T^* , and it covers the full length of the Fermi surface for $T > T^*$. In particular, in analogy to the temperature dependence of the Fermi arc length, the low-temperature Fermi arc length in the underdoped regime increases with increasing doping, and then it evolves into a continuous contour in momentum space near the end of the superconducting dome. The theory also predicts an almost linear doping dependence of the Fermi arc length.

PACS numbers: 74.25.Jb, 74.20.Mn, 74.72.Kf, 74.20.-z, 74.72.-h

I. INTRODUCTION

In the conventional superconductors², an energy gap exists in the electronic energy spectrum only below the superconducting (SC) transition temperature T_c , which is corresponding to the energy for breaking a Cooper pair of the charge carriers and creating two excited states. However, in cuprate superconductors above T_c but below a temperature T^* , an energy gap called the normal-state pseudogap exists³⁻⁶. Although the SC gap has a domelike shape of the doping dependence⁷, the magnitude of the normal-state pseudogap is much larger than that of the SC gap in the underdoped regime³⁻⁶, then it smoothly decreases upon increasing doping, and seems to merge with the SC gap in the overdoped regime, eventually disappearing together with superconductivity at the end of the SC dome⁵. Since many of the unusual physical properties of cuprate superconductors have often been attributed to particular characteristics of the low-energy excitations determined by the electronic structure⁵⁻⁷, the normal-state pseudogap observed in the excitation spectrum as a suppression of the spectral weight is thought to be key to understanding the mechanism of superconductivity.

During the last two decades, the angle-resolved photoemission spectroscopy (ARPES) has been emerged as a powerful tool for studying the electronic structure of cuprate superconductors, since it is a direct method for probing the momentum dependence of the SC gap and the locus in the momentum space where the quasiparticle excitations are gapless⁷. In spite of the nonconventional SC mechanism, the ARPES experimental results have unambiguously established the Bogoliubov-quasiparticle nature of the sharp SC quasiparticle peak in cuprate superconductors in the overdoped regime⁸, then the SC coherence of the low energy quasiparticle excitation is well fitted by a simple Bardeen-Cooper-Schrieffer (BCS)

formalism² with a d-wave SC gap. However, the pseudogap state is particularly obvious in the underdoped regime³⁻⁶, this leads to that the physical properties of cuprate superconductors in the underdoped regime exhibit a number of the anomalous properties^{3,5-7,9-13}. In particular, the ARPES experimental data show that in the underdoped regime, although the normal-state of cuprate superconductors is metallic, the part of the Fermi surface is gapped out by the normal-state pseudogap, then the low-energy electron excitations occupy disconnected segments called as the Fermi arcs located at the nodal region in the Brillouin zone^{9,10}. Moreover, in corresponding to the doping and temperature dependence of the normal-state pseudogap, the essential feature of the evolution of the Fermi arc length with doping and temperature has been established now⁹⁻¹³: (1) the Fermi arc in the underdoped regime increases in length with temperatures, till at about the normal-state pseudogap crossover temperature T^* , then it covers the full length of the Fermi surface (a continuous contour in momentum space) for the temperature $T > T^{*9-11}$; (2) the Fermi arc increases its length as a function of doping¹³, and then it evolves into a continuous contour in momentum space near the end of the SC dome. In particular, the experimental data indicate both the particle-hole symmetry breaking and the pronounced spectral broadening due to the presence of the normal-state pseudogap, which reflect the spatial symmetry breaking without long-range order at the opening of the normal-state pseudogap¹⁴⁻¹⁶. It is thus established that the low-energy quasiparticle excitations at the Fermi energy dramatically change with doping and temperature, and have a close relation to the normal-state pseudogap.

Although the main features of the particle-hole asymmetry electronic state in cuprate superconductors and the related doping and temperature dependence of the Fermi arc length are well-established by now⁹⁻¹⁶, their full understanding is still a challenging issue. In our

recent work¹⁷, the interplay between the SC gap and normal-state pseudogap in cuprate superconductors has been studied based on the kinetic energy driven SC mechanism¹⁸, where the charge carriers interact directly through the kinetic energy by exchanging spin excitations, then this microscopic interaction provides a natural explanation of both the origin of the normal-state pseudogap state in the particle-hole channel and the pairing mechanism for superconductivity in the particle-particle channel¹⁷. In this paper, we study the low-energy electronic structure of cuprate superconductors along with this line¹⁷. We evaluate explicitly the electron spectral function by taking into account the interplay between the SC gap and normal-state pseudogap, and then qualitatively reproduce the main features of the ARPES measurements on cuprate superconductors^{9–15}, including the doping and temperature dependence of the Fermi arc length.

The rest of this paper is organized as follows. We present the basic formalism in Section II, while the quantitative characteristics of the particle-hole asymmetry electronic state are discussed in Section III, where we show that the particle-hole asymmetry electronic state and the related doping and temperature dependence of the Fermi arc length are intriguingly related to the emergence of the normal-state pseudogap in the particle-hole channel. Finally, we give a summary in Section IV.

II. THEORETICAL FRAMEWORK

In cuprate superconductors, the single common feature is the presence of the CuO₂ plane⁷, and it seems evident that the unusual behavior is dominated by this plane. Very soon after the discovery of superconductivity in cuprate superconductors, it has been argued that the essential physics of the doped CuO₂ plane is contained in the t - J model on a square lattice¹⁹,

$$H = -t \sum_{i\hat{\eta}\sigma} C_{i\sigma}^\dagger C_{i+\hat{\eta}\sigma} + t' \sum_{i\hat{\tau}\sigma} C_{i\sigma}^\dagger C_{i+\hat{\tau}\sigma} + \mu \sum_{i\sigma} C_{i\sigma}^\dagger C_{i\sigma} + J \sum_{i\hat{\eta}} \mathbf{S}_i \cdot \mathbf{S}_{i+\hat{\eta}}, \quad (1)$$

supplemented by an important on-site local constraint $\sum_{\sigma} C_{i\sigma}^\dagger C_{i\sigma} \leq 1$ to remove the double occupancy, where the summation is over all sites i , and for each i , over its nearest-neighbors $\hat{\eta}$ or the next nearest-neighbors $\hat{\tau}$, $C_{i\sigma}^\dagger$ and $C_{i\sigma}$ are electron operators that respectively create and annihilate electrons with spin σ , $\mathbf{S}_i = (S_i^x, S_i^y, S_i^z)$ are spin operators, and μ is the chemical potential. For a proper treatment of the electron single occupancy local constraint in the t - J model (1), a charge-spin separation (CSS) fermion-spin theory^{20,21} has been proposed, where a spin-up annihilation (spin-down annihilation) operator for the physical electron is given by a composite operator as $C_{i\uparrow} = h_{i\uparrow}^\dagger S_i^-$ ($C_{i\downarrow} = h_{i\downarrow}^\dagger S_i^+$), with the spinful fermion

operator $h_{i\sigma} = e^{-i\Phi_{i\sigma}} h_i$ that keeps track of the charge degree of freedom of the electron together with some effects of spin configuration rearrangements due to the presence of the doped hole itself (charge carrier), while the spin operator S_i describes the spin degree of freedom of the electron, then the electron single occupancy local constraint is satisfied in analytical calculations. In this CSS fermion-spin representation, the t - J model (1) can be rewritten as^{20,21},

$$H = t \sum_{i\hat{\eta}} (h_{i+\hat{\eta}\uparrow}^\dagger h_{i\uparrow} S_i^+ S_{i+\hat{\eta}}^- + h_{i+\hat{\eta}\downarrow}^\dagger h_{i\downarrow} S_i^- S_{i+\hat{\eta}}^+) - t' \sum_{i\hat{\tau}} (h_{i+\hat{\tau}\uparrow}^\dagger h_{i\uparrow} S_i^+ S_{i+\hat{\tau}}^- + h_{i+\hat{\tau}\downarrow}^\dagger h_{i\downarrow} S_i^- S_{i+\hat{\tau}}^+) - \mu \sum_{i\sigma} h_{i\sigma}^\dagger h_{i\sigma} + J_{\text{eff}} \sum_{i\hat{\eta}} \mathbf{S}_i \cdot \mathbf{S}_{i+\hat{\eta}}, \quad (2)$$

where $J_{\text{eff}} = (1 - \delta)^2 J$, and the doping concentration $\delta = \langle h_{i\sigma}^\dagger h_{i\sigma} \rangle = \langle h_i^\dagger h_i \rangle$.

As in the conventional superconductors², the SC-state in cuprate superconductors is also characterized by the Cooper pairs, forming SC quasiparticles²². However, as a natural consequence of the unconventional SC mechanism that is responsible for the high SC transition temperatures¹⁹, the Cooper pair in cuprate superconductors has a dominant d-wave symmetry^{7,22}. In this case, one of the main concerns in the field of superconductivity in cuprate superconductors is about the origin of the d-wave Cooper pairs. From the experimental side, it has been well established that the antiferromagnetic short-range correlation coexists with the SC-state in the whole SC regime^{23–27}, which provides a clear link between the pairing mechanism and magnetic excitation. On the theoretical hand, we have developed a kinetic energy driven SC mechanism¹⁸ based on the t - J model (2), where the charge carrier interaction directly from the kinetic energy by exchanging spin excitations induces a d-wave charge carrier pairing state in the particle-particle channel, then the electron Cooper pairs originating from the charge carrier pairing state are due to the charge-spin recombination, and their condensation reveals the SC ground-state. Moreover, this SC-state is controlled by both the SC gap and quasiparticle coherence, which leads to that the maximal SC transition temperature occurs around the optimal doping, and then decreases in both the underdoped and overdoped regimes. This microscopic SC theory gives a consistent description of the physical properties of cuprate superconductors, including the doping and temperature dependence of the microwave conductivity²⁸, the extinction of the quasiparticle scattering interference²⁹, and the doping dependence of the Meissner effect³⁰. In particular, it has been shown recently that besides the pairing mechanism in the particle-particle channel provided by the charge carrier interaction directly from the kinetic energy by exchanging spin excitations, this same microscopic interaction also induces the normal-state pseudogap state in the particle-hole channel¹⁷. Based on this work¹⁷, we³¹

have discussed the doping dependence of the specific-heat of cuprate superconductors, and shown that the striking behavior of the specific-heat humplike anomaly near T_c in the underdoped regime can be attributed to the

emergence of the normal-state pseudogap. Following our previous discussions^{17,18}, the full charge carrier diagonal and off-diagonal Green's functions of the t - J model (2) in the SC-state can be obtained as,

$$g(\mathbf{k}, \omega) = \frac{1}{\omega - \xi_{\mathbf{k}} - \Sigma_1^{(h)}(\mathbf{k}, \omega) - \bar{\Delta}_h^2(\mathbf{k})/[\omega + \xi_{\mathbf{k}} + \Sigma_1^{(h)}(\mathbf{k}, -\omega)]}, \quad (3a)$$

$$\Gamma^\dagger(\mathbf{k}, \omega) = -\frac{\bar{\Delta}_h(\mathbf{k})}{[\omega - \xi_{\mathbf{k}} - \Sigma_1^{(h)}(\mathbf{k}, \omega)][\omega + \xi_{\mathbf{k}} + \Sigma_1^{(h)}(\mathbf{k}, -\omega)] - \bar{\Delta}_h^2(\mathbf{k})}, \quad (3b)$$

respectively, where $\xi_{\mathbf{k}} = Zt\chi_1\gamma_{\mathbf{k}} - Zt'\chi_2\gamma'_{\mathbf{k}} - \mu$ is the mean-field charge carrier spectrum with the spin correlation functions $\chi_1 = \langle S_i^+ S_{i+\hat{\eta}}^- \rangle$ and $\chi_2 = \langle S_i^+ S_{i+\hat{\tau}}^- \rangle$, $\gamma_{\mathbf{k}} = (1/Z) \sum_{\hat{\eta}} e^{i\mathbf{k} \cdot \hat{\eta}}$, $\gamma'_{\mathbf{k}} = (1/Z) \sum_{\hat{\tau}} e^{i\mathbf{k} \cdot \hat{\tau}}$, and Z is the number of the nearest-neighbor or next nearest-neighbor sites on a square lattice. The effective charge carrier pair gap $\bar{\Delta}_h(\mathbf{k}) = \Sigma_2^{(h)}(\mathbf{k}, \omega = 0)$, therefore it is closely related to the charge carrier self-energy $\Sigma_2^{(h)}(\mathbf{k}, \omega)$ in the *particle-particle channel*¹⁸, and can be expressed explicitly as a d-wave form $\bar{\Delta}_h(\mathbf{k}) = \bar{\Delta}_h \gamma_{\mathbf{k}}^{(d)}$ with $\gamma_{\mathbf{k}}^{(d)} = (\cos k_x - \cos k_y)/2$, while the effective charge carrier pair gap parameter $\bar{\Delta}_h$ and the charge carrier self-energy $\Sigma_1^{(h)}(\mathbf{k}, \omega)$ in the *particle-hole channel* have been given in Ref. 17. In this case, the Fermi energy is determined by the pole of the Green's function (3). In particular, $\Sigma_1^{(h)}(\mathbf{k}, \omega)$ can be written as¹⁷ $\Sigma_1^{(h)}(\mathbf{k}, \omega) = [2\bar{\Delta}_{pg}(\mathbf{k})]^2/[\omega + M_{\mathbf{k}}]$ with the effective normal-state pseudogap $\bar{\Delta}_{pg}(\mathbf{k})$ and the energy spectrum $M_{\mathbf{k}}$, which reflects that the effective normal-state pseudogap $\bar{\Delta}_{pg}(\mathbf{k})$ originates from $\Sigma_1^{(h)}(\mathbf{k}, \omega)$ ¹⁷. In this case, the imaginary part of $\Sigma_1^{(h)}(\mathbf{k}, \omega)$ can be ob-

tained as $\text{Im}\Sigma_1^{(h)}(\mathbf{k}, \omega) = -\pi[2\bar{\Delta}_{pg}(\mathbf{k})]^2\delta(\omega + M_{\mathbf{k}})$. This imaginary part is defined as a momentum dependence of the characteristic scattering rate (then the characteristic lifetime), and the type of this imaginary part is an intrinsic property of the electronic state of cuprate superconductors, since it has been used to provide a robust fit for the electron spectrum and spatially inhomogeneous differential conductances³².

It has been shown that the d-wave charge carrier pairing state in the particle-particle channel originating from the kinetic energy by exchanging the spin excitations also leads to form a d-wave electron Cooper pairing state¹⁸. For discussions of the electronic structure in the SC-state, we need to calculate the electron diagonal Green's function $G(i - j, t - t') = \langle \langle C_{i\sigma}(t); C_{j\sigma}^\dagger(t') \rangle \rangle$, which is a convolution of the spin Green's function $D^{(0)-1}(\mathbf{k}, \omega) = (\omega^2 - \omega_{\mathbf{k}}^2)/B_{\mathbf{k}}$ and charge carrier diagonal Green's function (3a) in the CSS fermion-spin theory³³, and can be evaluated in terms of the spectral representation as,

$$G(\mathbf{k}, \omega) = \frac{1}{2N} \sum_{\mathbf{p}} \frac{B_{\mathbf{p}+\mathbf{k}}}{\omega_{\mathbf{p}+\mathbf{k}}} \int_{-\infty}^{+\infty} \frac{d\omega'}{2\pi} A_h(\mathbf{p}, \omega') \left[\frac{n_F(\omega') + n_B(\omega_{\mathbf{p}+\mathbf{k}})}{\omega + \omega' - \omega_{\mathbf{p}+\mathbf{k}}} + \frac{1 + n_B(\omega_{\mathbf{p}+\mathbf{k}}) - n_F(\omega')}{\omega + \omega' + \omega_{\mathbf{p}+\mathbf{k}}} \right], \quad (4)$$

where the charge carrier spectral function $A_h(\mathbf{k}, \omega) = -2\text{Im}G(\mathbf{k}, \omega)$, while the spin excitation spectrum $\omega_{\mathbf{k}}$ and the function $B_{\mathbf{k}}$ have been given in Ref. 33. This convolution of the spin Green's function and charge carrier Green's function reflects the charge-spin recombination³⁴. The electronic state in a solid is characterized by its energy dispersion as well as the characteristic lifetime (then the characteristic scattering rate) of an electron placed into such a state. This state is just represented by the electron Green's function (4), while the electron spectral function $A(\mathbf{k}, \omega)$ is directly related

to the analytically continued electron Green's function (4) as $A(\mathbf{k}, \omega) = -2\text{Im}G(\mathbf{k}, \omega)$, and can be obtained explicitly in terms of the electron Green's function (4) as,

$$A(\mathbf{k}, \omega) = \frac{1}{2N} \sum_{\mathbf{p}} \frac{B_{\mathbf{p}+\mathbf{k}}}{\omega_{\mathbf{p}+\mathbf{k}}} \{ A_h(\mathbf{p}, \omega_{\mathbf{p}+\mathbf{k}} - \omega) [n_F(\omega_{\mathbf{p}+\mathbf{k}} - \omega) + n_B(\omega_{\mathbf{p}+\mathbf{k}})] + A_h(\mathbf{p}, -\omega_{\mathbf{p}+\mathbf{k}} - \omega) \times [1 + n_B(\omega_{\mathbf{p}+\mathbf{k}}) - n_F(-\omega_{\mathbf{p}+\mathbf{k}} - \omega)] \}. \quad (5)$$

In particular, this spectral function (5) is measurable via the ARPES technique and can provide an important information about quasiparticle excitations⁷.

III. PARTICLE-HOLE ASYMMETRY ELECTRONIC STATE DUE TO THE PRESENCE OF THE NORMAL-STATE PSEUDOGAP

In this section, we discuss the particle-hole asymmetry electronic state in cuprate superconductors and the related doping and temperature dependence of the Fermi arc length in the presence of the normal-state pseudogap. In our recent work¹⁷, we have shown that there is a coexistence of the SC gap and normal-state pseudogap in the whole SC dome, where the effective charge carrier pair gap parameter $\bar{\Delta}_h$ has a domelike shape of the doping dependence, while the magnitude of the effective normal-state pseudogap parameter $\bar{\Delta}_{pg}$ is particularly large in the underdoped regime, then it smoothly decreases with increasing doping, and eventually disappears together with superconductivity at the end of the SC dome. In particular, this $\bar{\Delta}_{pg}$ is closely related to the charge carrier quasiparticle coherent weight Z_{hF} as¹⁷ $Z_{hF}^{-1} = 1 + [2\bar{\Delta}_{pg}(\mathbf{k})]^2/M_{\mathbf{k}}^2|_{\mathbf{k}=[\pi,0]}$, this is why Z_{hF} grows linearly with doping^{18,33}. We have therefore established a relationship between $\bar{\Delta}_{pg}$ and Z_{hF} , and the obtained evolution of both $\bar{\Delta}_{pg}$ and Z_{hF} with doping is qualitative agreement with the corresponding experimental data^{5,35,36}. Since the SC-state in the kinetic energy driven SC mechanism is controlled by both the SC gap and quasiparticle coherence¹⁸, and in this sense, the normal-state pseudogap is a necessary ingredient for superconductivity. Moreover, $\bar{\Delta}_{pg}$ is also temperature dependent, and it vanishes at the normal-state pseudogap crossover temperature T^* , while this T^* as a function of doping has a similar doping dependence as $\bar{\Delta}_{pg}$ ¹⁷. Furthermore, by calculation of the ratio of the effective charge carrier pair gap parameter $\bar{\Delta}_h$ and the charge carrier pair gap parameter Δ_h , we¹⁷ have also obtained the coupling (interaction) strength V_{eff} , and the result shows clearly that V_{eff} smoothly decreases upon increasing doping from a strong-coupling case in the underdoped regime to a weak-coupling side in the overdoped regime. In particular, we¹⁷ find that all T^* , $\bar{\Delta}_{pg}$, and V_{eff} show the same trend with doping, i.e., $T^* \sim \bar{\Delta}_{pg} \sim V_{eff}$, while such a relationship among T^* , $\bar{\Delta}_{pg}$, and V_{eff} has been observed experimentally on cuprate superconductors³⁷.

A. Doping and temperature dependence of the Fermi arc length

In the following discussions, we discuss the evolution of the Fermi arc length with doping and temperature. The notion of the Fermi surface is one of the characteristic concepts in the field of condensed matter physics, and it plays a crucial role in the understanding of interacting electron systems. In Fig. 1, we show the maps of the spectral intensity at the Fermi energy for (a) the underdoping $\delta = 0.09$, (b) the optimal doping $\delta = 0.15$, (c) the overdoping $\delta = 0.21$, and (d) the doping near the end of the SC dome $\delta = 0.26$ with parameters

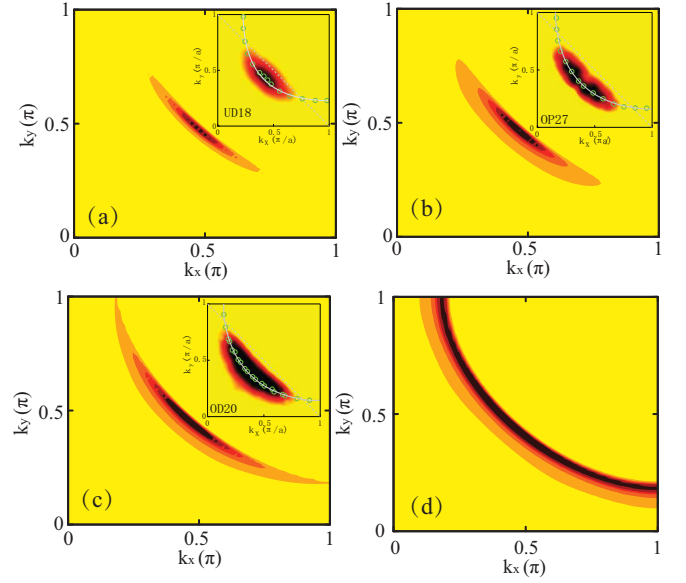


FIG. 1: (Color online) The doping evolution of the spectral intensity maps at the Fermi energy for (a) $\delta = 0.09$, (b) $\delta = 0.15$, (c) $\delta = 0.21$, and (d) $\delta = 0.26$ with $t/J = 2.5$, $t'/t = 0.3$, and $J = 110\text{meV}$ in $T = 2.55\text{K}$. Inset: the corresponding experimental data of $\text{Ca}_{2-x}\text{Na}_x\text{CuO}_2\text{Cl}_2$ at the underdoping, the optimal doping, and the overdoping, respectively, taken from Ref. 13.

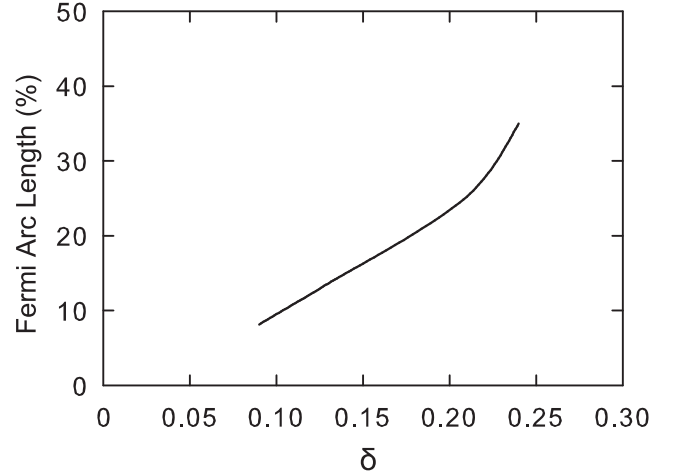


FIG. 2: The Fermi arc length as a function of doping in $T = 2.55\text{K}$ with $t/J = 2.5$, $t'/t = 0.3$, and $J = 110\text{meV}$. On the y axis, 0% is the node and 100% is the antinode.

$t/J = 2.5$, $t'/t = 0.3$, and $J = 110\text{meV}$ in temperature $T = 2.55\text{K}$. For comparison, the corresponding experimental results¹³ of $\text{Ca}_{2-x}\text{Na}_x\text{CuO}_2\text{Cl}_2$ for the underdoping, the optimal doping, and the overdoping are also shown in Fig. 1(a), Fig. 1(b), and Fig. 1(c), respectively (inset). It is shown clearly that our present theoretical results capture all qualitative features of the doping dependence of the Fermi arc length observed experimentally on cuprate superconductors¹³. In the underdoped regime, the Fermi surface does not form a continuous

contour in momentum space, instead, it is broken into disconnected arcs. However, this Fermi arc increases its length as a function of doping, and there is a tendency towards to form a continuous contour in momentum space. This tendency is particularly obvious in the overdoped regime, where the Fermi arc becomes flat, and then it covers the full length of the Fermi surface at the doping near the end of the SC dome [see Fig. 1(d)], in qualitative agreement with experimental data¹³. Moreover, we have fitted our present results, and found that the Fermi arc length rise almost linearly with doping. This anticipated result is plotted in Fig. 2.

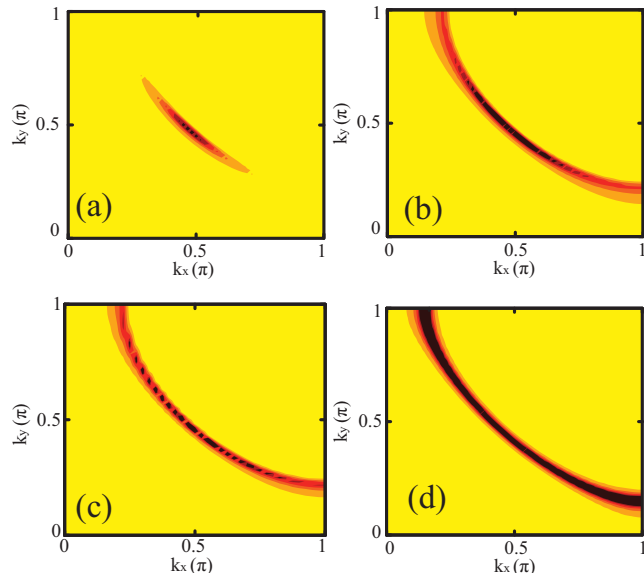


FIG. 3: (Color online) The temperature evolution of the spectral intensity maps at the Fermi energy for $\delta = 0.09$ in (a) $T = 2.55\text{K}$, (b) $T = 57.45\text{K}$, (c) $T = 70.2\text{K}$, and (d) $T = 242.55\text{K}$ with $t/J = 2.5$, $t'/t = 0.3$, and $J = 110\text{meV}$.

To analyze the evolution of the spectral intensity at the Fermi energy with temperature, we have made a series of calculations for the spectral density at the Fermi energy with different temperatures, and the results of the maps of the spectral density at the Fermi energy for $\delta = 0.09$ with $t/J = 2.5$, $t'/t = 0.3$, and $J = 110\text{meV}$ in (a) $T = 2.55\text{K}$, (b) $T = 57.45\text{K}$, (c) $T = 70.2\text{K}$, and (d) $T = 242.55\text{K}$ are plotted in Fig. 3. Within the kinetic energy driven SC mechanism, the calculated $T_c = 67.6\text{K}$ and $T^* = 238.7\text{K}$, respectively, for $\delta = 0.09$. For $T < T_c$, the Fermi arc shrinks to the nodal region [see Fig. 3(a)]. However, with increasing temperatures, in particular, for $T > T^*$, the Fermi surface forms a continuous contour in momentum space [see Fig. 3(d)]. To show this temperature dependence of the Fermi arc length clearly, the result for the extracted Fermi arc length as a function of temperature for $\delta = 0.09$ with $t/J = 2.5$, $t'/t = 0.3$, and $J = 110\text{meV}$ is plotted in Fig. 4 in comparison with the corresponding experimental result¹⁰ of $\text{Bi}_2\text{Sr}_2\text{CaCu}_2\text{O}_{8+\delta}$ (inset). Our result shows that the Fermi arc length is a linear function of

temperature in the temperature range $T_c < T < T^*$, i.e., it increases linearly with increasing temperatures, which is in good agreement with experimental data^{9–11} in this temperature range. However, below T_c , although the Fermi arc length monotonically increases up to T_c , the Fermi arc length is a nonlinear function of temperature. We have also noted that a possible nonlinear temperature dependence of the Fermi arc length seems to have been observed¹¹ experimentally on $(\text{Bi,Pb})_2\text{Sr}_2\text{CuO}_6$.

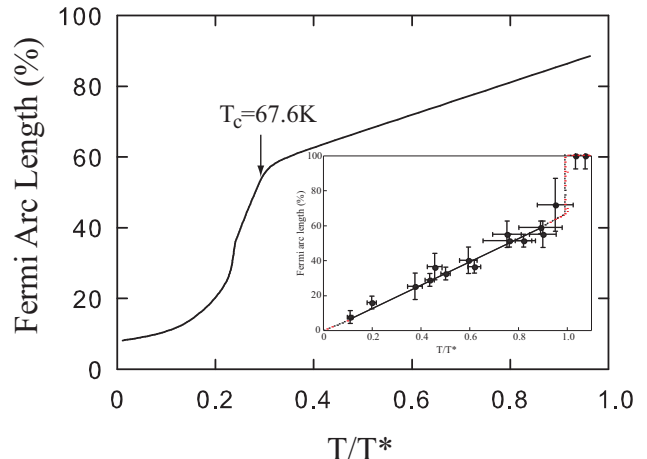


FIG. 4: The Fermi arc length as a function of temperature for $\delta = 0.09$ with $t/J = 2.5$, $t'/t = 0.3$, and $J = 110\text{meV}$. Inset: the corresponding experimental result of $\text{Bi}_2\text{Sr}_2\text{CaCu}_2\text{O}_{8+\delta}$ taken from Ref. 10. On the y axis, 0% is the node and 100% is the antinode.

B. Particle-hole asymmetry electronic state

Now we turn to discuss the particle-hole asymmetry electronic state in the presence of the normal-state pseudogap. In the conventional superconductors^{2,14}, a particle-hole symmetric energy gap opens from the normal-state dispersion because of the homogeneous superconductivity, where there is an alignment between the Fermi crossing k_F and the back-bending or the saturation momentum of the dispersion in the gapped states. However, the recent improvements in the resolution of the ARPES experiments allowed for an experimental verification of the particle-hole symmetry breaking in the normal-state pseudogap state of cuprate superconductors^{14,15}, in particular, this particle-hole asymmetry electronic state observed from the ARPES experiments is manifested itself by the nonalignment between the Fermi crossing k_F and the back-bending or the saturation momentum of the dispersion in the gapped states. For a better understanding of the nature of the particle-hole asymmetry electronic state in cuprate superconductors^{14,15}, we have performed a calculation for the spectral function $A(\mathbf{k}, \omega)$ (5) along the direction $[\pi, -\pi] \rightarrow [\pi, 0] \rightarrow [\pi, \pi]$ in different temperatures, and

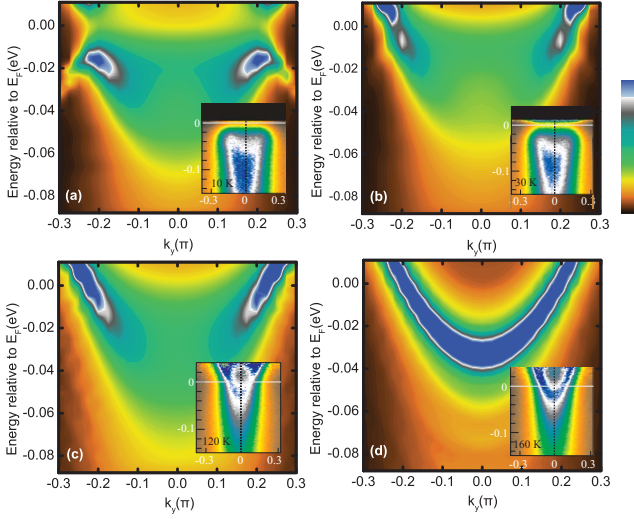


FIG. 5: (Color online) The maps of the electron spectral function as a function of momentum along the direction $[\pi, -\pi] \rightarrow [\pi, 0] \rightarrow [\pi, \pi]$ for $\delta = 0.09$ with $t/J = 2.5$, $t'/t = 0.3$, and $J = 110\text{meV}$ in (a) $T = 2.55\text{K}$, (b) $T = 57.45\text{K}$, (c) $T = 70.2\text{K}$, and (d) $T = 242.55\text{K}$. Inset: the corresponding experimental results of $\text{Pb}_{0.55}\text{Bi}_{1.5}\text{Sr}_{1.6}\text{La}_{0.4}\text{CuO}_{6+\delta}$ taken from Ref. 14.

the results of the maps of $A(\mathbf{k}, \omega)$ as a function of momentum for $\delta = 0.09$ with $t/J = 2.5$, $t'/t = 0.3$, and $J = 110\text{meV}$ in (a) $T = 2.55\text{K}$, (b) $T = 57.45\text{K}$, (c) $T = 70.2\text{K}$, and (d) $T = 242.55\text{K}$ are plotted in Fig. 5 in comparison with the corresponding experimental data¹⁴ of $\text{Pb}_{0.55}\text{Bi}_{1.5}\text{Sr}_{1.6}\text{La}_{0.4}\text{CuO}_{6+\delta}$ (inset). For $T > T^*$, the spectrum as a function of momentum has a parabolic dispersion of the intensity maximum with two clear Fermi level crossings at k_{F1} and k_{F2} momenta and a bottom reaching $E_{\text{bot}} \sim 0.02\text{eV}$ at $[\pi, 0]$ point. In this case, the normal-state of the system is a Landau Fermi liquid similar to that of an ordinary metal. However, for $T < T^*$, the spectral weight centroid is transferred towards a higher binding energy, where although the spectral weight of the quasiparticle excitation is strongly suppressed at low temperatures, the intensity maximum of the spectrum can be defined and traced as function of momentum. In particular, this characteristic feature of the spectrum is still persists even in the SC-state ($T < T_c$). To show this point clearly, we plot the positions of the low energy quasiparticle peaks in $A(\mathbf{k}, \omega)$ as a function of momentum along the direction $[\pi, -\pi] \rightarrow [\pi, 0] \rightarrow [\pi, \pi]$ for $\delta = 0.09$ with $t/J = 2.5$, $t'/t = 0.3$, and $J = 110\text{meV}$ in $T = 2.55\text{K}$ (solid line) and $T = 242.55\text{K}$ (dashed line) in Fig. 6 in comparison with the corresponding experimental results¹⁴ of $\text{Pb}_{0.55}\text{Bi}_{1.5}\text{Sr}_{1.6}\text{La}_{0.4}\text{CuO}_{6+\delta}$ (inset). Obviously, for $T > T^*$, the spectrum is gapless at the Fermi crossings k_{F1} and k_{F2} , and the quasiparticle peaks at low energies disperse parabolically with momentum. However, for $T < T^*$, the dispersion at the relatively low energy shows the back-bending at k_{G1} and k_{G2} momenta, while the band bottom at $[\pi, 0]$ point has

been pushed far away from the normal-state E_{bot} appeared for $T > T^*$. In this case, the spectrum is fully gapped, and no back-bending appears at k_{F1} and k_{F2} . These results are in qualitative agreement with these observed from ARPES experimental measurements^{14,15} on $\text{Pb}_{0.55}\text{Bi}_{1.5}\text{Sr}_{1.6}\text{La}_{0.4}\text{CuO}_{6+\delta}$.

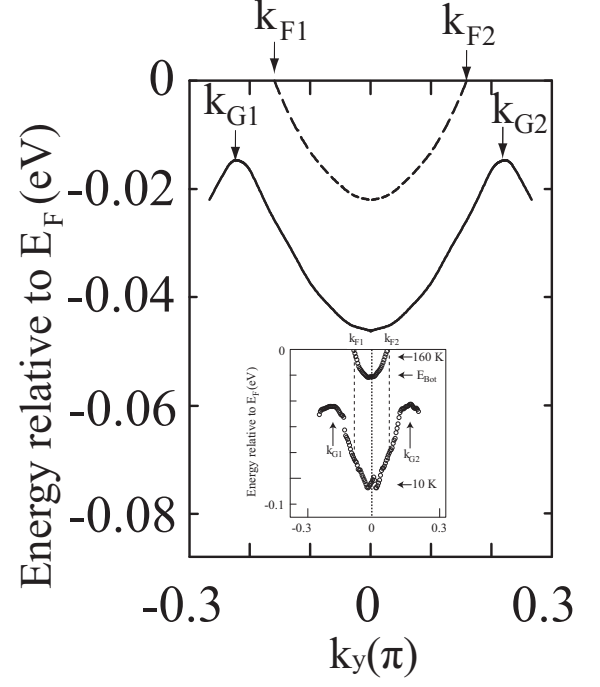


FIG. 6: The positions of the lowest energy quasiparticle peaks in the electron spectral function as a function of momentum along the direction $[\pi, -\pi] \rightarrow [\pi, 0] \rightarrow [\pi, \pi]$ for $\delta = 0.09$ with $t/J = 2.5$, $t'/t = 0.3$, and $J = 110\text{meV}$ in $T = 2.55\text{K}$ (solid line) and $T = 242.55\text{K}$ (dashed line). Inset: the corresponding experimental results of $\text{Pb}_{0.55}\text{Bi}_{1.5}\text{Sr}_{1.6}\text{La}_{0.4}\text{CuO}_{6+\delta}$ taken from Ref. 14.

Furthermore, we have also discussed the doping dependence of the particle-hole asymmetry electronic state. In Fig. 7, we plot the maps of the spectral function $A(\mathbf{k}, \omega)$ as a function of momentum along the direction $[\pi, -\pi] \rightarrow [\pi, 0] \rightarrow [\pi, \pi]$ for (a) $\delta = 0.09$, (b) $\delta = 0.15$, (c) $\delta = 0.21$, and (d) $\delta = 0.26$ with $t/J = 2.5$, $t'/t = 0.3$, and $J = 110\text{meV}$ in $T = 2.55\text{K}$, where the behavior of the evolution of the particle-hole asymmetry electronic state with doping is very similar to that of the doping dependence of the particle-hole asymmetry electronic state shown in Fig. 5. For the doping near the end of the SC dome, the maxima of the spectral function have an approximately parabolic dispersion [see Fig. 7(d)]. In this case, the quasiparticle excitations are gapless, and the dispersion crosses the Fermi level at two momenta k_{F1} and k_{F2} . However, the dispersion rises to a minimum binding energy and then bends back in the underdoping [see Fig. 7(a)], where there is an energy gap in the quasiparticle excitations. In particular, this back-bending occurs at two momenta k_{G1} and k_{G2} , which are separated

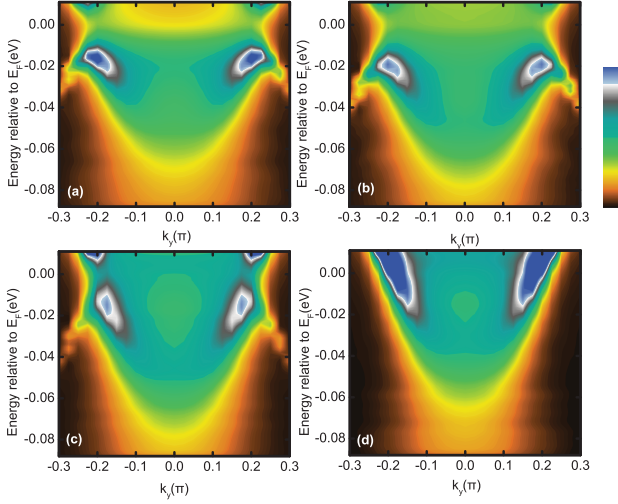


FIG. 7: (Color online) The maps of the electron spectral function as a function of momentum along the direction $[\pi, -\pi] \rightarrow [\pi, 0] \rightarrow [\pi, \pi]$ for (a) $\delta = 0.09$, (b) $\delta = 0.15$, (c) $\delta = 0.21$, and (d) $\delta = 0.26$ with $t/J = 2.5$, $t'/t = 0.3$, and $J = 110\text{meV}$ in $T = 2.55\text{K}$.

from the corresponding Fermi crossing points k_{F1} and k_{F2} , as summarized in Fig. 8. Moreover, the gap size and the distance between the k_{G1} and k_{F1} (then k_{G2} and k_{F2}) decrease with increasing doping.

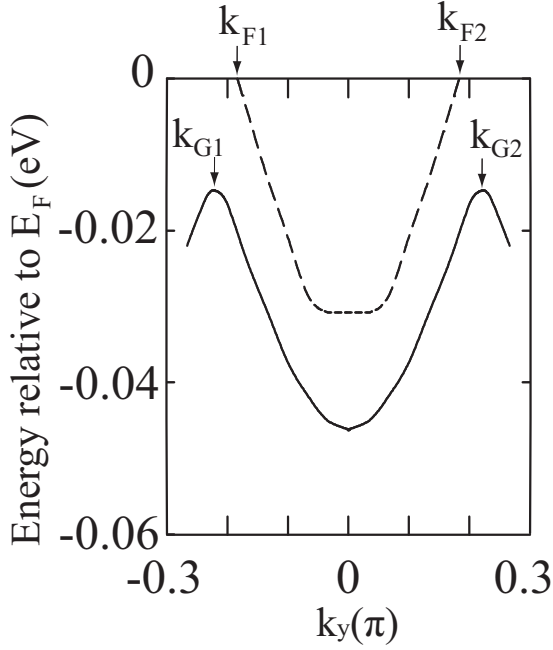


FIG. 8: The positions of the lowest energy quasiparticle peaks in the electron spectral function as a function of momentum along the direction $[\pi, -\pi] \rightarrow [\pi, 0] \rightarrow [\pi, \pi]$ for $\delta = 0.09$ (solid line) and $\delta = 0.26$ (dashed line) with $t/J = 2.5$, $t'/t = 0.3$, and $J = 110\text{meV}$ in $T = 2.55\text{K}$.

A natural question is why the particle-hole asymmetry electronic state in cuprate superconductors and

the related doping and temperature dependence of the Fermi arc length can be described qualitatively within the framework of the kinetic energy driven superconductivity¹⁸. The reason is that the emergence of the doping and temperature dependence of the normal-state pseudogap¹⁷. This follows a fact that in the framework of the kinetic energy driven SC mechanism, besides the pairing mechanism in the particle-particle channel provided by the charge carrier interaction directly from the kinetic energy by exchanging spin excitations, this same microscopic interaction also induces a normal-state pseudogap state in the particle-hole channel¹⁷ as mentioned above. This normal-state pseudogap opens at the Fermi energy for $T < T^*$, which competes with superconductivity by suppressing the spectral weight of the quasiparticle excitation. Since the magnitude of the normal-state pseudogap decreases with increasing doping and temperature¹⁷, this leads to that the strength of the suppression for the spectral weight also decreases with increasing doping and temperature. In this case, the particle-hole asymmetry electronic state and the related doping and temperature dependence of the Fermi arc length are a natural consequence due to the presence of the normal-state pseudogap in the particle-hole channel. In the extremely low temperatures ($T \sim 0$), as a result of the strong suppression for the spectral weight in the underdoped regime, the electronic state breaks the particle-hole symmetry, where the majority contribution for the electron spectrum comes from the nodal region, i.e., the most low-energy states are located around the nodal region, forming the Fermi arcs. However, the strength of this suppression decreases with increasing doping, which leads to that the Fermi arc length increases with increasing doping. In particular, for the doping near the end of the SC dome, the normal-state pseudogap is negligible¹⁷, i.e., $\bar{\Delta}_{pg} \approx 0$. In this case, the full charge carrier diagonal and off-diagonal Green's functions (3) are reduced as a simple d-wave BCS formalism³¹,

$$g(\mathbf{k}, \omega) = \frac{U_{\mathbf{hk}}^2}{\omega - E_{\mathbf{hk}}} + \frac{V_{\mathbf{hk}}^2}{\omega + E_{\mathbf{hk}}}, \quad (6a)$$

$$\Gamma^\dagger(\mathbf{k}, \omega) = -\frac{\bar{\Delta}_{\mathbf{h}}(\mathbf{k})}{2E_{\mathbf{hk}}} \left(\frac{1}{\omega - E_{\mathbf{hk}}} - \frac{1}{\omega + E_{\mathbf{hk}}} \right), \quad (6b)$$

although the pairing mechanism in the particle-particle channel is driven by the kinetic energy by exchanging spin excitations, where the charge carrier quasiparticle coherence factors $U_{\mathbf{hk}}^2 = (1 + \xi_{\mathbf{k}}/E_{\mathbf{hk}})/2$ and $V_{\mathbf{hk}}^2 = (1 - \xi_{\mathbf{k}}/E_{\mathbf{hk}})/2$, and the charge carrier quasiparticle spectrum $E_{\mathbf{hk}} = \sqrt{\xi_{\mathbf{k}}^2 + |\bar{\Delta}_{\mathbf{h}}(\mathbf{k})|^2}$. It is thus similar to the conventional superconductors^{2,14}, in this simple d-wave BCS formalism (6), the Fermi arc covers the full length of the Fermi surface, and an alignment between the Fermi crossing k_F and the back-bending in the electronic state appears. This is why the SC coherence of the low energy quasiparticle excitation and the related physical properties in the heavily overdoped regime are well described by a simple d-wave BCS formalism^{8,31,33}.

On the other hand, in the normal-state pseudogap phase ($T_c < T < T^*$), the charge carrier pair gap $\bar{\Delta}_h = 0$, and then the full charge carrier diagonal Green's function (3) can be reduced as^{17,31},

$$g(\mathbf{k}, \omega) = \frac{\alpha_{1\mathbf{k}}^{(n)}}{\omega - E_{h\mathbf{k}}^+} + \frac{\alpha_{2\mathbf{k}}^{(n)}}{\omega - E_{h\mathbf{k}}^-}, \quad (7)$$

where the charge carrier quasiparticle coherence factors $\alpha_{1\mathbf{k}}^{(n)} = (E_{h\mathbf{k}}^+ + M_{\mathbf{k}})/(E_{h\mathbf{k}}^+ - E_{h\mathbf{k}}^-)$ and $\alpha_{2\mathbf{k}}^{(n)} = -(E_{h\mathbf{k}}^- + M_{\mathbf{k}})/(E_{h\mathbf{k}}^+ - E_{h\mathbf{k}}^-)$, while the dispersion has two branches, $E_{h\mathbf{k}}^+ = [\xi_{\mathbf{k}} - M_{\mathbf{k}} + \sqrt{(\xi_{\mathbf{k}} + M_{\mathbf{k}})^2 + 16\bar{\Delta}_{pg}^2(\mathbf{k})}]/2$ and $E_{h\mathbf{k}}^- = [\xi_{\mathbf{k}} - M_{\mathbf{k}} - \sqrt{(\xi_{\mathbf{k}} + M_{\mathbf{k}})^2 + 16\bar{\Delta}_{pg}^2(\mathbf{k})}]/2$. In this normal-state pseudogap phase, the particle-hole symmetry is broken due to the presence the normal-state pseudogap. However, with increasing temperatures, in particular, for $T > T^*$, both the normal-state pseudogap $\bar{\Delta}_{pg} = 0$ and the charge carrier pair gap $\bar{\Delta}_h = 0$, and in this case, the full charge carrier diagonal Green's function (3) is reduced as,

$$g(\mathbf{k}, \omega) = \frac{1}{\omega - \xi_{\mathbf{k}}}. \quad (8)$$

In this case, the normal-state is a particle-hole symmetry Landau Fermi liquid similar to that of an ordinary metal, and the Fermi arc turns into a continuous contour in momentum space.

IV. CONCLUSIONS

In this paper, we have studied the particle-hole asymmetry electronic state in cuprate superconductors and the related doping and temperature dependence of the Fermi arc length within the framework of the kinetic energy driven SC mechanism. By taking into account the

interplay between the SC gap and normal-state pseudogap, we have reproduced qualitatively the essential feature of the evolution of the Fermi arc length with doping and temperature. Our results show that the particle-hole asymmetry electronic state in cuprate superconductors is a natural consequence due to the presence the normal-state pseudogap in the particle-hole channel. The Fermi arc length increases with increasing temperature below T^* , and it covers the full length of the Fermi surface for $T > T^*$. In particular, in analogy to the temperature dependence of the Fermi arc length, the low-temperature Fermi arc length in the underdoped regime increases with increasing doping, and then it evolves into a continuous contour in momentum space near the end of the SC dome. The theory also predicts an almost linear doping dependence of the Fermi arc length, which should be verified by further experiments. Since the knowledge of the particle-hole asymmetry electronic state is of considerable importance as a test for the microscopic SC mechanism in cuprate superconductors, the qualitative agreement between the present theoretical results and ARPES experimental data also provides an important confirmation of the nature of the SC phase of cuprate superconductors as a coexistence of the kinetic energy driven d-wave SC-state in the particle-particle channel and the normal-state pseudogap state in the particle-hole channel in the whole SC dome.

Acknowledgments

This work was supported by the funds from the Ministry of Science and Technology of China under Grant Nos. 2011CB921700 and 2012CB821403, and the National Natural Science Foundation of China under Grant No. 11074023.

* To whom correspondence should be addressed, E-mail: spfeng@bnu.edu.cn.

² J. R. Schrieffer, *Theory of Superconductivity* (Addison-Wesley, San Francisco, 1964).

³ B. Batlogg, H.Y. Hwang, H. Takagi, R.J. Cava, H.L. Kao, and J. Kwo, *Physica C* **235-240**, 130 (1994).

⁴ H. Ding, T. Yokoya, J. C. Campuzano, T. Takahashi, M. Randeria, M. R. Norman, T. Mochiku, K. Kadowaki, and J. Giapintzakis, *Nature* **382**, 51 (1996); A. G. Loeser, Z.-X. Shen, D. S. Dessau, D. S. Marshall, C. H. Park, P. Fournier, and A. Kapitulnik, *Science* **273**, 325 (1996).

⁵ See, e.g., S. Hüfner, M. A. Hossain, A. Damascelli, and G. A. Sawatzky, *Rep. Prog. Phys.* **71**, 062501 (2008), and references therein.

⁶ See, e.g., Tom Timusk and Bryan Statt, *Rep. Prog. Phys.* **62**, 61 (1999), and references therein.

⁷ See, e.g., Andrea Damascelli, Zahid Hussain, and Zhi-Xun

Shen, *Rev. Mod. Phys.* **75**, 473 (2003), and references therein.

⁸ W. S. Lee, I. M. Vishik, K. Tanaka, D. H. Lu, T. Sasagawa, N. Nagaosa, T. P. Devereaux, Z. Hussain and Z.-X. Shen, *Nature* **450**, 81 (2007); H. Matsui, T. Sato, T. Takahashi, S. C. Wang, H. B. Yang, H. Ding, T. Fujii, T. Watanabe, and A. Matsuda, *Phys. Rev. Lett.* **90**, 217002 (2003); J. C. Campuzano, H. Ding, M. R. Norman, M. Randeria, A. F. Bellman, T. Yokoya, T. Takahashi, H. Katayama-Yoshida, T. Mochiku, and K. Kadowaki, *Phys. Rev. B* **53**, R14737 (1996).

⁹ M. R. Norman, H. Ding, M. Randeria, J. C. Campuzano, T. Yokoya, T. Takeuchi, T. Takahashi, T. Mochiku, K. Kadowaki, P. Guptasarma, and D. G. Hinks, *Nature* **392**, 157 (1998).

¹⁰ A. Kanigel, M. R. Norman, M. Randeria, U. Chatterjee, S. Souma, A. Kaminski, H. M. Fretwell, S. Rosenkranz, M.

- Shi, T. Sato, T. Takahashi, Z. Z. Li, H. Raffy, K. Kadowaki, D. Hinks, L. Ozyuzer, and J. C. Campuzano, *Nature Phys.* **2**, 447 (2006); U. Chatterjee, M. Shi, D. Ai, J. Zhao, A. Kanigel, S. Rosenkranz, H. Raffy, Z. Z. Li, K. Kadowaki, D. G. Hinks, Z. J. Xu, J. S. Wen, G. Gu, C. T. Lin, H. Claus, M. R. Norman, M. Randeria, and J. C. Campuzano, *Nature Phys.* **6**, 99 (2010).
- ¹¹ K. Nakayama, T. Sato, Y. Sekiba, K. Terashima, P. Richard, T. Takahashi, K. Kudo, N. Okumura, T. Sasaki, and N. Kobayashi, *Phys. Rev. Lett.* **102**, 227006 (2009).
 - ¹² Takeshi Kondo, Rustem Khasanov, Tsunehiro Takeuchi, Jörg Schmalian, and Adam Kaminski, *Nature* **457**, 296 (2009).
 - ¹³ Jian-Qiao Meng, M. Brunner, K.-H. Kim, H.-G. Lee, S.-I. Lee, J. S. Wen, Z. J. Xu, G. D. Gu, and G.-H. Gweon, *Phys. Rev. B* **84**, 060513(R) (2011).
 - ¹⁴ Makoto Hashimoto, Rui-Hua He, Kiyohisa Tanaka, Jean-Pierre Testaud, Worawat Meevasana, Rob G. Moore, Donghui Lu, Hong Yao, Yoshiyuki Yoshida, Hiroshi Eisaki, Thomas P. Devereaux, Zahid Hussain, and Zhi-Xun Shen, *Nature Phys.* **6**, 414 (2010).
 - ¹⁵ Rui-Hua He, M. Hashimoto, H. Karapetyan, J. D. Koralek, J. P. Hinton, J. P. Testaud, V. Nathan, Y. Yoshida, Hong Yao, K. Tanaka, W. Meevasana, R. G. Moore, D. H. Lu, S.-K. Mo, M. Ishikado, H. Eisaki, Z. Hussain, T. P. Devereaux, S. A. Kivelson, J. Orenstein, A. Kapitulnik, and Z.-X. Shen, *Science* **331**, 1579 (2011).
 - ¹⁶ R. Daou, J. Chang, David LeBoeuf, Olivier Cyr-Choinière, Francis Laliberté, Nicolas Doiron-Leyraud, B. J. Ramshaw, Ruixing Liang, D. A. Bonn, W. N. Hardy, and Louis Taillefer, *Nature* **463**, 519 (2010); Y. Kohsaka, C. Taylor, P. Wahl, A. Schmidt, Jinhwan Lee, K. Fujita, J. W. Alldredge, K. McElroy, Jinho Lee, H. Eisaki, S. Uchida, D.-H. Lee, and J. C. Davis, *Nature* **454**, 1072 (2008).
 - ¹⁷ Shiping Feng, Huaisong Zhao, and Zheyu Huang, *Phys. Rev. B* **85**, 054509 (2012).
 - ¹⁸ Shiping Feng, *Phys. Rev. B* **68**, 184501 (2003); Shiping Feng, Tianxing Ma, and Huaiming Guo, *Physica C* **436**, 14 (2006).
 - ¹⁹ P. W. Anderson, in *Frontiers and Borderlines in Many Particle Physics*, edited by R. A. Broglia and J. R. Schrieffer (North-Holland, Amsterdam, 1987), p. 1; *Science* **235**, 1196 (1987).
 - ²⁰ Shiping Feng, Jihong Qin, and Tianxing Ma, *J. Phys.: Condens. Matter* **16**, 343 (2004).
 - ²¹ See, e.g., the review, Shiping Feng, Huaiming Guo, Yu Lan, and Li Cheng, *Int. J. Mod. Phys. B* **22**, 3757 (2008).
 - ²² See, e.g., C. C. Tsuei and J. R. Kirtley, *Rev. Mod. Phys.* **72**, 969 (2000).
 - ²³ K. Yamada, C. H. Lee, K. Kurahashi, J. Wada, S. Wakimoto, S. Ueki, H. Kimura, Y. Endoh, S. Hosoya, G. Shirane, R. J. Birgeneau, M. Greven, M. A. Kastner, and Y. J. Kim, *Phys. Rev. B* **57**, 6165 (1998).
 - ²⁴ Pengcheng Dai, H. A. Mook, R. D. Hunt, and F. Doğan, *Phys. Rev. B* **63**, 054525 (2001).
 - ²⁵ C. Stock, W. J. L. Buyers, R. A. Cowley, P. S. Clegg, R. Coldea, C. D. Frost, R. Liang, D. Peets, D. Bonn, W. N. Hardy, and R. J. Birgeneau, *Phys. Rev. B* **71**, 024522 (2005).
 - ²⁶ M. Arai, T. Nishijima, Y. Endoh, T. Egami, S. Tajima, K. Tomimoto, Y. Shiohara, M. Takahashi, A. Garrett, and S. M. Bennington, *Phys. Rev. Lett.* **83**, 608 (1999).
 - ²⁷ Ph. Bourges, B. Keimer, S. Pailhès, L.P. Regnault, Y. Sidis, and C. Ulrich, *Physica C* **424**, 45 (2005); S. M. Hayden, H. A. Mook, Pengcheng Dai, T. G. Perring, and F. Doğan, *Nature* **429**, 531 (2004).
 - ²⁸ Zhi Wang, Huaiming Guo, and Shiping Feng, *Physica C* **468**, 1078 (2008); Zhi Wang and Shiping Feng, *Phys. Rev. B* **80**, 174507 (2009).
 - ²⁹ Zhi Wang, Bin Liu, and Shiping Feng, *Phys. Lett. A* **374**, 3084 (2010).
 - ³⁰ Shiping Feng, Zheyu Huang, and Huaisong Zhao, *Physica C* **470**, 1968 (2010); Zheyu Huang, Huaisong Zhao, and Shiping Feng, *Phys. Rev. B* **83**, 144524 (2011).
 - ³¹ Huaisong Zhao, Lulin Kuang, and Shiping Feng, *Physica C* **478**, 49 (2012).
 - ³² I. M. Vishik, E. A. Nowadnick, W. S. Lee, Z. X. Shen, B. Moritz, T. P. Devereaux, K. Tanaka, T. Sasagawa, and T. Fujii, *Nature Phys.* **5**, 718 (2009); J. W. Alldredge, Jinho Lee, K. McElroy, M. Wang, K. Fujita, Y. Kohsaka, C. Taylor, H. Eisaki, S. Uchida, P. J. Hirschfeld, and J. C. Davis, *Nature Phys.* **4**, 319 (2008).
 - ³³ Huaiming Guo and Shiping Feng, *Phys. Lett. A* **361**, 382 (2007); Yu Lan, Jihong Qin, and Shiping Feng, *Phys. Rev. B* **76**, 014533 (2007).
 - ³⁴ P.W. Anderson, *Phys. Rev. Lett.* **67**, 2092 (1991); *Science* **288**, 480 (2000).
 - ³⁵ D. L. Feng, D. H. Lu, K. M. Shen, C. Kim, H. Eisaki, A. Damascelli, R. Yoshizaki, J.-i. Shimoyama, K. Kishio, G. D. Gu, S. Oh, A. Andrus, J. ÓDonnell, J. N. Eckstein, and Z.-X. Shen, *Science* **289**, 277 (2000).
 - ³⁶ H. Ding, J. R. Engelbrecht, Z. Wang, J. C. Campuzano, S.-C. Wang, H.-B. Yang, R. Rogan, T. Takahashi, K. Kadowaki, and D. G. Hinks, *Phys. Rev. Lett.* **87**, 227001 (2001).
 - ³⁷ A. A. Kordyuk, V. B. Zabolotnyy, D. V. Evtushinsky, D. S. Inosov, T. K. Kim, B. Büchner, and S. V. Borisenko, *Eur. Phys. J. Special Topics* **188**, 153 (2010).